Available online at www.sciencedirect.com
SCIENCE DIRECT®
Journal of Computational Physics 215 (2006) 642–660
JOURNAL OF COMPUTATIONAL PHYSICS
www.elsevier.com/locate/jcp

A new absorbing layer for elastic waves

Daniel Appelö *,[1], Gunilla Kreiss [2]

Department of Numerical Analysis and Computer Science, Royal Institute of Technology, Lindstedsv. 3, Stockholm S-100 44, Sweden

Received 26 February 2005; received in revised form 2 November 2005; accepted 8 November 2005
Available online 19 December 2005

Abstract

A new perfectly matched layer (PML) for the simulation of elastic waves in anisotropic media on an unbounded domain is constructed. Theoretical and numerical results, showing that the stability properties of the present layer are better than previously suggested layers, are presented. In addition, the layer can be formulated with fewer auxiliary variables than the split-field PML.

MSC: 65M06; 65M12; 35L05; 74J05; 74S30

Keywords: Perfectly matched layers; PML; Absorbing layers; Elastic waves

1. Introduction

The perfectly matched layer (PML) model was introduced by Berenger [1] in the context of computational electro-magnetics. Berenger introduced the additional degrees of freedom needed for the perfect matching by splitting one of the physical fields, and his model is therefore often referred to as the split-field model.

In [2] Collino and Tsogka showed how to construct a PML model by the split-field approach for a general hyperbolic system. They applied their theory to the equations of linear elasticity in an anisotropic medium. The perfect matching property follows directly from the construction. However, there is no guarantee that the solution in the layer is damped with time. In fact, there are many examples of split-field PML models supporting growing solutions, see e.g. [3–5]. The original PML model for Maxwell's equations, suggested by Berenger, supports linearly growing modes [6]. Several methods have been devised to remove growing modes e.g. filtering [4,5], introduction of a complex frequency shift [7], and addition of stabilizing parameters (with loss of the perfect matching) [8,9].

* Corresponding author.
E-mail addresses: appelo@nada.kth.se (D. Appelö), gunillak@nada.kth.se (G. Kreiss).
URLs: www.nada.kth.se/~appelo (D. Appelö), www.nada.kth.se/~gunillak (G. Kreiss).
[1] Supported by the Swedish research council grant no. VR2004-2371.
[2] Supported in part by the Swedish research council grant no. VR2004-2371.

0021-9991/$ - see front matter © 2005 Elsevier Inc. All rights reserved.
doi:10.1016/j.jcp.2005.11.006

Stability of the split-field PML model has been studied in numerous works, see e.g. [10–12,3,6,7]. One particularly interesting approach is that of Bécache et al. [3], who use plane wave analysis to establish necessary conditions for weak stability of the general split-field model. This condition is violated in the cases where exponential growth is observed, [3–5]. The fact that the condition is only necessary is illustrated by numerical experiments where exponentially growing solutions are observed. By a detailed study of the dispersion relation, Bécache et al. establish a set of conditions, on the coefficients of elasticity, which are necessary and sufficient for weak stability. The results of Bécache et al. explain the observed exponential growth when the split-field PML is used for some orthotropic media, but they do not give suggestions on how it can be removed.

In this paper we consider PML models for the equations of linear elasticity in an anisotropic medium. There exist many PML models for the simulations of elastic waves in both isotropic and anisotropic material, e.g. [2,13–15], which are of the split-field type. In many layers growing modes are observed. We derive a new PML model using a method suggested by Hagstrom [16]. Hagstrom's method is based on modification of the *modal solutions* of a symmetric or strongly hyperbolic system.

For each specific problem, parameters in a candidate PML model derived with Hagstrom's method much be chosen (yielding a new PML model for each specific problem) such that the solution inside the layer is damped exponentially in space. Here we show how to choose parameters for the particular problem of linear elasticity in an anisotropic medium. Even if the solution is damped in space there is no guarantee that it will be stable in time. We show how the techniques in [3] can be used to analyze the stability of our PML.

The main contributions of this paper is contained in Sections 5.1–5.3 and 6. The paper is organized as follows. In Section 2 definitions for well-posedness and stability are stated.

In Section 3 we introduce the equations of linear elastodynamics in anisotropic heterogeneous media. We introduce the dispersion relation and describe how plane waves and slowness curves can be used to describe wave propagation in different media. Here we also present the materials that will be considered throughout the paper. These materials are the same as in [3].

In Section 4 we introduce the split-field PML model suggested by Collino and Tsogka [2]. We also review some of the stability results from [3] for the split-field PML and discuss their choice of materials.

In Section 5 we first review the formulation of a modal PML, for a general hyperbolic system, including several free parameters [16]. In Section 5.1 we apply the model to the equations of linear elasticity. This is the first time the modal PML has been used for these equations. We briefly describe the geometrical interpretation of the parameters in the model. We conclude that only one additional parameter can be used for the equations of linear elasticity. The resulting model is analyzed by the perturbation techniques introduced in [3]. We present new theoretical results showing that our PML model has better stability properties than previous split-field models. Also, the model is formulated with fewer variables than previous models. We conclude Section 5 with a discussion of the well-posedness of the new layer model. We show that the model is weakly well-posed.

In Section 6 we present numerical experiments, showing the efficiency of the modal PML for the simulation of elastic waves on unbounded domains. We also present simulations illustrating the improved stability properties.

In Section 7 we summarize and conclude.

2. Preliminaries

In this paper stability and well-posedness of perfectly matched layers used for simulation of elastic waves on unbounded domains will be discussed. We start by defining what we mean by stability and well-posedness (see [17]).

Consider the Cauchy problem for systems

$$\begin{aligned} &\frac{\partial u}{\partial t} = P\left(\frac{\partial}{\partial x}\right)u, \quad x \in \mathbb{R}^n, t \geqslant 0, \\ &u(x,0) = u_0(x), \quad x \in \mathbb{R}^n, \end{aligned} \tag{1}$$

with initial data in L^2.

Definition 1 (Well-posedness). The Cauchy problem (1) is

(i) *well-posed*: if the solutions satisfy $\|u(\cdot,t)\|_{L^2} \leqslant K e^{\kappa t}\|u(\cdot,0)\|_{L^2}$;
(ii) *weakly well-posed*: if the solutions satisfy $\|u(\cdot,t)\|_{L^2} \leqslant K e^{\kappa t}\|u(\cdot,0)\|_{H^s}$ for some positive integer s but not for $s = 0$.

A necessary and sufficient condition for weak well-posedness is that all eigenvalues λ_j of the symbol $P(ik)$ satisfy

$$\Re\{\lambda_j(P(ik))\} \leqslant \kappa, \tag{2}$$

κindependent of k.

Definition 2 (Stability). We say that the Cauchy problem (1) is

(i) *strongly stable*: if the solutions satisfy an estimate $\|v(\cdot,t)\|_{L^2} \leqslant K\|v_0(\cdot)\|_{L^2}$;
(ii) *weakly stable*: if the solutions satisfy an estimate $\|v(\cdot,t)\|_{L^2} \leqslant K(1+t)^s\|v_0(\cdot)\|_{H^s}$, where $s > 0$.

A sufficient condition for weak stability is

$$\Re\{\lambda(P(ik))\} \leqslant 0. \tag{3}$$

If, in addition to (2), $P(ik)$ can be diagonalized by $S(ik)$ with $|S(ik)|$ and $|S^{-1}(ik)|$ uniformly bounded, then the problem is well-posed.

3. Elastic waves

The equations of motion in a continuum can be written, with Einstein's convention of summation,

$$\rho\frac{\partial^2 u_i}{\partial t^2} = \frac{\partial \sigma_{ij}}{\partial x_j}, \tag{4}$$

if body forces are neglected. We work in two dimensions and therefore the indices i, j assume the values $\{1, 2\}$. Here ρ is the density, u_1 and u_2 are the displacements and σ_{ij} is the stress tensor, which is related to the tensor of deformation

$$\varepsilon_{ij} = \frac{1}{2}\left(\frac{\partial u_i}{\partial x_j} + \frac{\partial u_j}{\partial x_i}\right),$$

by Hooke's law

$$\sigma_{ij} = c_{ijkl}\varepsilon_{kl}, \tag{5}$$

where c_{ijkl} is the tensor of elastic constants. Using the symmetry of the tensors σ_{ij}, ε_{kl} and c_{ijkl} and the scheme

$$(11) \leftrightarrow (1), \quad (22) \leftrightarrow (2), \quad (12) \leftrightarrow (21) \leftrightarrow (3),$$

which replaces two indices by one and four indices by 2, we can write (5)

$$\sigma_n = c_{nm}\varepsilon_m, \quad n, m = 1, 2, 3,$$

where $c_{mn} = c_{nm}$.

Using characteristic lengths, time, etc. of the problem we can non-dimensionalize it. For the construction of a PML it is convenient to reformulate the second order formulation (4) as a first order system

$$\frac{\partial v}{\partial t} - A_1\frac{\partial v}{\partial x_1} - A_2\frac{\partial v}{\partial x_2} = 0. \tag{6}$$

By introducing the velocity fields $v_1 = \partial_t \bar{u}_1$, $v_2 = \partial_t u_2$ and denoting $v_3 = \bar{\sigma}_1$, $v_4 = \bar{\sigma}_2$, $v_5 = \bar{\sigma}_3$, the non-dimensionalized version of Eq. (4) can be reformulated as a first order system (the velocity–stress formulation) with

$$A_1 = \begin{bmatrix} 0 & 0 & 1 & 0 & 0 \\ 0 & 0 & 0 & 0 & 1 \\ c_{11} & c_{13} & 0 & 0 & 0 \\ c_{12} & c_{23} & 0 & 0 & 0 \\ c_{13} & c_{33} & 0 & 0 & 0 \end{bmatrix}, \quad A_2 = \begin{bmatrix} 0 & 0 & 0 & 0 & 1 \\ 0 & 0 & 0 & 1 & 0 \\ c_{13} & c_{12} & 0 & 0 & 0 \\ c_{23} & c_{22} & 0 & 0 & 0 \\ c_{33} & c_{23} & 0 & 0 & 0 \end{bmatrix}. \tag{7}$$

Here the bared variables are the non-dimensionalized variables. In the reminder of this paper we will drop the bars on the non-dimensionalized time and space coordinates, denoting them t and x.

For the reminder of this paper we will consider an orthotropic medium with principal axis coinciding with the x_1 and x_2-axis. For such a medium we have that $c_{13} = c_{23} = 0$. For simplicity we will also take ρ to be 1.

In this paper we consider the same orthotropic materials as in [3]. These materials where chosen to illustrate three different types of instabilities occurring when the split-field PML for anisotropic elasticity is used. The materials are defined by the values of the coefficients of elasticity, see Table 1.

3.1. Plane waves and slowness curves

To analyze the wave propagation properties of (6) it is useful to consider the particular solution

$$v(x,t) = V e^{i(\omega t - k\cdot x)}, \tag{8}$$

where $k \in \mathbb{R}^2$ is the wave vector, $\omega \in \mathbb{R}$ is the (circular) frequency and V is the amplitude. By inserting the solution (8) into (6) we get a solvability condition, usually referred to as the dispersion relation

$$F(\omega, k) \equiv \det(\omega I + k_1 A_1 + k_2 A_2) = 0. \tag{9}$$

The solutions $\omega(k)$ are the eigenvalues of the matrix $-(k_1 A_1 + k_2 A_2)$, i.e. $i\omega_j = \lambda_j(P(ik))$.

For waves in an orthotropic medium (with $\rho = 1$), (9) is

$$\begin{aligned} \widetilde{F}_0(\omega, k) \equiv \omega[&\omega^4 - ((c_{33} + c_{11})k_1^2 + (c_{33} + c_{22})k_2^2)\omega^2 + (c_{11}c_{22} - c_{12}^2 - 2c_{12}c_{33})k_1^2 k_2^2 + c_{11}c_{33}k_1^4 + c_{22}c_{33}k_2^4] \\ &= 0. \end{aligned} \tag{10}$$

It should be noted that the eigenvalue $w(k) = 0$ is introduced when (4) is rewritten as a first order system (6). This eigenvalue corresponds to a non-propagating mode. We also define

$$F_0(\omega, k) \equiv \widetilde{F}_0(\omega, k)/\omega = 0, \tag{11}$$

which is the dispersion relation of the second order formulation (4). As in [3], we will refer to the solutions of (11) as physical modes and to the zero eigenvalue as a non-physical mode. Other useful quantities are the unit wave vector, K, the phase velocity, $\mathscr{V}_p$ and the slowness vector $S = (S_1, S_2)$, defined by

$$K = \frac{k}{|k|}, \quad \mathscr{V}_p = \frac{\omega}{|k|}, \quad S = \frac{k}{\omega}. \tag{12}$$

Being homogeneous in ω and k, (11) can be rewritten as

$$F_0(1, S) = 0. \tag{13}$$

Table 1
Elasticity coefficients of the orthotropic materials

Material	c_{11}	c_{22}	c_{33}	c_{12}
I	4	20	2	3.8
II	20	20	2	3.8
III	4	20	2	7.5
VI	10	20	6	2.5
V	30	6	1.5	9.9

The wave propagation properties of a certain medium can be understood by drawing the slowness curve, defined by the points in the S plane satisfying (13). The slowness curve for the orthotropic media considered here (see Fig. 1) will consist of two branches corresponding to the quasi-longitudinal and quasi-shear waves, see [18]. Each branch is related to two roots $\pm\omega(k)$ of (11).

For each of these branches, the group velocity, $\mathscr{V}_g$, is defined by

$$\mathscr{V}_g(k) = \nabla_k \omega(k). \tag{14}$$

If we also assume that $c_{33} \neq c_{11}$ and $c_{33} \neq c_{22}$, the two branches will not intersect and then the group velocity can be expressed as

$$\mathscr{V}_g(k) = \nabla_k \omega(k) = -\left(\frac{\partial F_0(\omega(k),k)}{\partial \omega}\right)^{-1} \nabla_k F_0(\omega(k),k), \tag{15}$$

i.e. the group velocity is normal to the slowness curve. For a detailed discussion of the physical interpretation of slowness curves, group velocity and energy transport in solids, see [18].

4. The split-field PML model

The split-field PML model was first formulated by Berenger [1] for Maxwell's equations. In [2], a split-field PML model for a general hyperbolic system has been introduced. For a PML model in a layer parallel to the x_2-axis, for the system (6), it can be written

$$\begin{aligned} &\frac{\partial v^1}{\partial t} + d(x_1)v^1 - A_1 \frac{\partial (v^1 + v^2)}{\partial x_1} = 0, \\ &\frac{\partial v^2}{\partial t} - A_2 \frac{\partial (v^1 + v^2)}{\partial x_2} = 0. \end{aligned} \tag{16}$$

By construction the number of variables in the split-field PML is doubled compared to the number of variables in the original system (6), i.e. for elastic waves the split-field PML is a system with 10 variables.

4.1. Stability of the split-field PML for orthotropic waves

In [3] the stability of the split-field PML was studied in detail. Here we list some of the results from [3], which are relevant to the discussion of our PML in the next section.

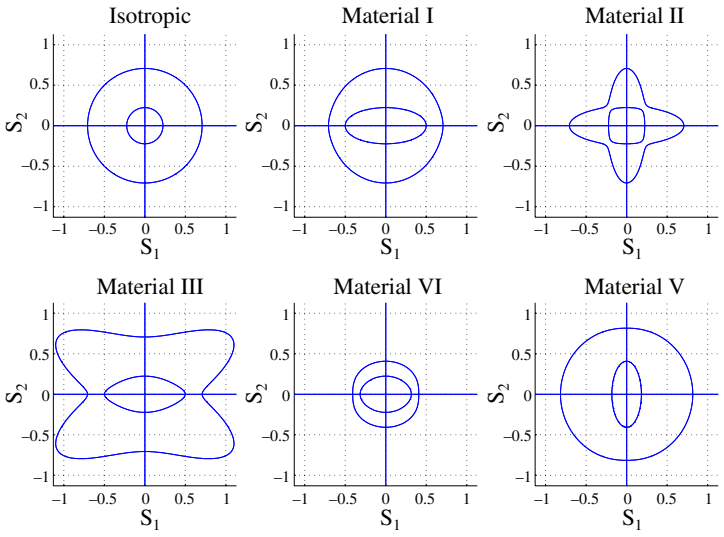

Fig. 1. Slowness curves for different materials.

In the reminder of this section we will consider a split-field PML parallel to the x_2-axis (see Eq. (16)) for the simulation of orthotropic waves. We will also assume d to be constant and positive.

Theorem 3 (Bécache et al. [3], Theorem 2). *Assume that the $m \times m$ system,*

$$u_t = A_1 u_{x_1} + A_2 u_{x_2}, \tag{17}$$

is strongly hyperbolic, and that the corresponding symbol has N_e non-zero and simple eigenvalues, and one zero eigenvalue of order $l_0 = m - N_e$. A necessary condition for weak stability of the split-field PML model (16) is that, for all physical modes of (17)

$$\forall K = (K_1, K_2) \text{ such that } |K| = 1, \quad S_1(K)\mathcal{V}_{g1}(K) \geqslant 0. \tag{18}$$

One can show that the condition (18) is also sufficient for stability, of the physical modes, at all sufficiently large frequencies, i.e. when $\varepsilon = d/|k|$ is small enough.

The geometric interpretation of Theorem 3 is that the first component of the slowness vector and the first component of the group velocity should point in the same direction, see Fig. 2. From the shape of the slowness curves in Fig. 1, it is easy to see that all materials except material III satisfy this high frequency stability criterion.

The fact that the condition (18) is not sufficient for stability of the split-field PML for certain materials has been illustrated by numerical experiments in [3]. In particular, when using the split-field PML for simulations in materials IV and V exponential growth in time was observed. The growth in time is slow compared to the instabilities observed when the high frequency stability condition is violated. Since they appear only after long time, they where not observed in [2].

By a detailed analysis of the dispersion relation for orthotropic media, Bécache et al. obtained necessary and sufficient conditions on the coefficients of elasticity. These conditions guarantee the stability of the split-field PML model. They are (Lemma 4, Lemma 5 and Theorem 5 in [3])

$$\begin{aligned} (c_{12} + 2c_{33})^2 &\leqslant c_{11}c_{22}, \\ (c_{12} + c_{33}) &\leqslant c_{11}c_{22} + c_{33}^2, \end{aligned} \tag{19}$$

and either of the conditions

$$(c_{12} + c_{33})^2 \leqslant (c_{11} - c_{33})(c_{22} - c_{33}), \tag{20}$$

$$(c_{11} + c_{33})(c_{12} + c_{33})^2 \geqslant (c_{11} - c_{22})(c_{11}c_{22} - c_{33}^2). \tag{21}$$

These conditions explain the observed instabilities for material IV and V. Material IV violates condition (19) and supports growing non-physical modes for high frequencies. Material V violates conditions (20)–(21) and supports growing physical modes at intermediate frequencies.

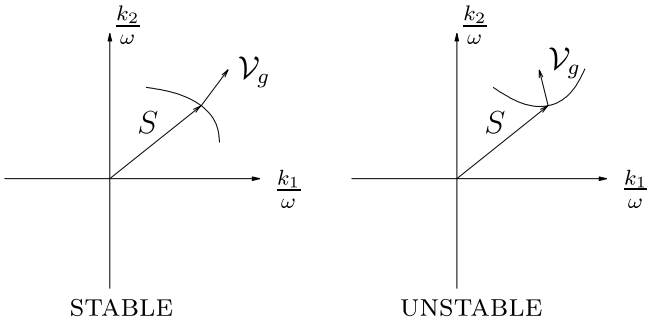

Fig. 2. Stable and unstable portions of the slowness curve.

5. The modal PML

We now consider the PML model for hyperbolic systems suggested by Hagstrom [16]. The model is obtained by modifying the *modal solutions* of the original system, so that the solution inside the layer is damped exponentially in space.

Again, consider the construction of a damping layer parallel with the x_2-axis starting at $x_1 = 0$. For the construction of the modal PML, the first step is to state the modal solutions of (6) by performing Laplace transform in time and Fourier transform in the x_2 direction. The modal solution is

$$\hat{v} = \mathrm{e}^{\lambda x_1}\hat{\psi}(s, \mathrm{i}k_2), \quad (-sI + \lambda A_1 + \mathrm{i}k_2 A_2)\hat{\psi}(s, \mathrm{i}k_2) = 0. \tag{22}$$

Inside the layer, the governing equations are constructed by the following ansatz for the modal solution:

$$\hat{v}_L = \mathrm{e}^{\lambda x_1 + \left(\frac{(\lambda-\gamma_1)}{s+\alpha_1+\alpha_0} - \gamma_0\right)\int_0^{x_1} d(z)\,\mathrm{d}z}\hat{\psi}(s, \mathrm{i}k_2). \tag{23}$$

The ansatz can, in principle, be formulated with arbitrary many parameters but for most hyperbolic systems the parameters α_0, α_1, γ_0, γ_1 will be sufficient. The damping function d is positive and smooth, taking the value zero at the interface $x_1 = 0$.

The governing equations inside the layer can be derived by taking the derivative with respect to x_1 of (23)

$$\frac{\partial}{\partial x_1}\hat{v}_L = \left(\lambda + \left(\frac{(\lambda-\gamma_1)}{s+\alpha_1+\alpha_0} - \gamma_0\right)d\right)\hat{v}_L.$$

This equality can be reformulated as

$$\lambda\hat{v}_L = \left(\frac{\partial}{\partial x_1} + d\gamma_0 - \frac{d(\frac{\partial}{\partial x_1} + d\gamma_0 - \gamma_1)}{s+\alpha_1+\alpha_0+d}\right)\hat{v}_L.$$

Now introduce the auxiliary variable $\hat{w}$ defined by

$$\frac{-(\frac{\partial}{\partial x_1} + d\gamma_0 - \gamma_1)}{s+\alpha_1+\alpha_0+d}\hat{v}_L = \hat{w}.$$

Insert λ in (22) and drop the subscript L

$$\begin{aligned} s\hat{v} &= A_1\left(\frac{\partial\hat{v}}{\partial x_1} + d(\gamma_0\hat{v} + \hat{w})\right) + \mathrm{i}k_2 A_2\hat{v}, \\ (s + d + \alpha_1 + \alpha_0)\hat{w} &+ \frac{\partial\hat{v}}{\partial x_1} + (d\gamma_0 - \gamma_1)\hat{v} = 0, \end{aligned}$$

inverting the transforms, the equations in the layer are finally obtained

$$\begin{aligned} \frac{\partial v}{\partial t} &= A_1\left(\frac{\partial v}{\partial x_1} + d(\gamma_0 v + w)\right) + A_2\frac{\partial v}{\partial x_2}, \\ \frac{\partial w}{\partial t} &+ (d + \bar{\alpha}_1 + \alpha_0)w + \frac{\partial v}{\partial x_1} + d\gamma_0 v - \bar{\gamma}_1 v = 0. \end{aligned} \tag{24}$$

Here $\bar{\gamma}_1$ can be taken to be a differential operator on the form $g\partial_{x_2}$, where g is a real scalar, $\bar{\alpha}_1$ will also be on the form $a\partial_{x_2}$ and γ_0 and α_0 are real scalars. Note that the layer will be perfectly matched for all $(\bar{\gamma}_1, \gamma_0, \bar{\alpha}_1, \alpha_0)$ so the main issue is to choose them so that the layer is damping.

5.1. Application of the modal PML to orthotropic waves

In [19] an analysis of the model (24) applied to the system defined by

$$A_1 = \begin{bmatrix} a_{11} & a_{12} \\ a_{12} & a_{22} \end{bmatrix}, \quad A_2 = \begin{bmatrix} b_{11} & b_{12} \\ b_{12} & b_{22} \end{bmatrix} \tag{25}$$

was presented. For this particular system, a necessary and sufficient condition for stability of the modal PML is that the slowness curves of the system (6)+(25) satisfies the condition (18) in the transformed coordinate system

$$S_1' = \frac{k_1}{\omega + \alpha_0 + ak_2} - g\frac{k_2}{\omega + \alpha_0 + ak_2} - \gamma_0, \quad S_2' = \frac{k_2}{\omega + \alpha_0 + ak_2}. \tag{26}$$

For a general system (6) this condition is only necessary.

The geometrical interpretation of the different parameters is that if g is non-zero, the slowness curve will be rotated around origin in the transformed system. The parameter γ_0 corresponds to displacement of the slowness curve in the S_1' direction. The parameter α_0 does not have an immediate geometrical interpretation but as we soon will see it can add extra stability to the PML.

Similar coordinate transforms have been used to construct stable PML models for the linearized Euler equations [9,20,21] and the shallow water equations [8]. However, in those works the authors explicitly perform a coordinate transformation of the system at hand, then derive the PML equations, and finally transform them back to the original coordinate system. With the modal PML we always work with the original variables and the transformed coordinate system is just a tool for determining the parameters in the model.

For material III there is no choice of parameter values for which the slowness curve in the transformed system (26) satisfies the condition (18). For materials I, II, IV and V the condition (18) is satisfied if and only if $\gamma_0 = g = a = 0$.

If we make that choice and apply the modal PML to the equations involving x_1 derivatives (propagating modes) the resulting equations of the PML become

$$\begin{aligned} &\frac{\partial v}{\partial t} = A_1\left(\frac{\partial v}{\partial x_1} + d(x_1)E_1 w_1\right) + A_2\frac{\partial v}{\partial x_2}, \\ &\frac{\partial w_1}{\partial t} + E_1^{\mathrm{T}}\frac{\partial v}{\partial x_1} + d(x_1)w_1 + \alpha_0 w_1 = 0. \end{aligned} \tag{27}$$

Here $E_1 w_1 = [w_{1,1}, w_{1,2}, w_{1,3}, 0, w_{1,4}]^{\mathrm{T}}$ ($w_{1,i}$ is the ith component of the vector w_1), $E_1^{\mathrm{T}} v_{x_1} = [v_1, v_2, v_3, v_5]_{x_1}^{\mathrm{T}}$ and α_0 is a small positive number. With this formulation we only have four auxiliary variables. Hence the system (27) contains only nine equations.

We note that the above choices of γ_0, g and a are necessary whenever the slowness curve(s) are centered around the origin. Examples of equations with this property are Euler's equations linearized at a quiescent state and Maxwell's equations, see [22]. Also the first order formulation of the (dispersive) wave equation in 2 or 3 dimensions and the shallow water equations linearized at a quiescent state with or without Coriolis forces have this property.

Including also the PML parallel to the x_1-axis, we get the full formulation

$$\begin{aligned} &\frac{\partial v}{\partial t} = A_1\left(\frac{\partial v}{\partial x_1} + d_1(x_1)E_1 w_1\right) + A_2\left(\frac{\partial v}{\partial x_2} + d_2(x_2)E_2 w_2\right), \\ &\frac{\partial w_1}{\partial t} + E_1^{\mathrm{T}}\frac{\partial v}{\partial x_1} + d_1(x_1)w_1 + \alpha_{01} w_1 = 0, \\ &\frac{\partial w_2}{\partial t} + E_2^{\mathrm{T}}\frac{\partial v}{\partial x_2} + d_2(x_2)w_2 + \alpha_{02} w_2 = 0. \end{aligned} \tag{28}$$

Here the matrix E_1 is defined as above, $E_2 w_2 = [w_{2,1}, w_{2,2}, 0, w_{2,3}, w_{2,4}]^{\mathrm{T}}$ and $E_1^{\mathrm{T}} v_{x_2} = [v_1, v_2, v_4, v_5]_{x_2}^{\mathrm{T}}$.

5.2. Stability of the modal PML for orthotropic waves

In this section we will see that the stability properties of the model (27) can always be made as good as for the split-field PML. For non-physical modes the stability at high frequencies will be better. The improved stability is due to the parameter α_0 which, in the context of computational electro magnetics, often is referred to as the complex frequency shift. It was first considered in [23] where it was introduced to make the PML model

satisfy causality conditions imposed by the Kramers-Kronig relations. It has also been shown that it removes the late time growth in PML formulations for Maxwell's equations [7].

In the reminder of this section we will assume that the physical eigenvalues of the second order formulation are simple and non-zero. As in [3] we consider d constant, and use the plane wave ansatz to obtain the dispersion relation of (27),

$$\widetilde{F}_m(\omega,k_1,k_2,d,\alpha_0)\equiv\omega F_0(\omega(\omega-\mathrm{i}d-\mathrm{i}\alpha_0),k_1(\omega-\mathrm{i}\alpha_0),k_2(\omega-\mathrm{i}d-\mathrm{i}\alpha_0))=0. \tag{29}$$

Here, F_0 is defined by (11). Comparing (29) with the dispersion relation of the split-field PML model (see [3]) we see that the dispersion relations are identical when $\alpha_0=0$. We thus have

Corollary 4. *Under the assumptions of Theorem 3, a necessary condition for stability of the PML model (27), with $\alpha_0=0$, is that all physical modes of (11) satisfy the condition on the orientation of the slowness curve (18).*

Having established a formal equivalence of the two PML models when $\alpha_0=0$, we turn to the case $\alpha_0>0$. The mode $\omega=0$ will not cause instability and it is sufficient to consider

$$F_m(\omega,k_1,k_2,d,\alpha_0)\equiv F_0(\omega(\omega-\mathrm{i}d-\mathrm{i}\alpha_0),k_1(\omega-\mathrm{i}\alpha_0),k_2(\omega-\mathrm{i}d-\mathrm{i}\alpha_0))=0. \tag{30}$$

Introducing

$$\varepsilon=\frac{d}{|k|},\quad \delta=\frac{\alpha_0}{|k|},\quad \mathscr{V}_{\mathrm{p}}=\frac{\omega}{|k|}, \tag{31}$$

we can rewrite (30) as

$$F_0(\mathscr{V}_{\mathrm{p}}(\mathscr{V}_{\mathrm{p}}-\mathrm{i}\varepsilon-\mathrm{i}\delta),K_1(\mathscr{V}_{\mathrm{p}}-\mathrm{i}\delta),K_2(\mathscr{V}_{\mathrm{p}}-\mathrm{i}\varepsilon-\mathrm{i}\delta))=0, \tag{32}$$

When $\varepsilon=\delta=0$, by homogeneity, (32) reduces to

$$\mathscr{V}_{\mathrm{p}}^4F_0(\mathscr{V}_{\mathrm{p}},K_1,K_2)=0.$$

The four zero modes will be referred to as non-physical modes and the other will be referred to as physical modes. The stability of the physical modes can be analyzed by a perturbation analysis for $\varepsilon<<1$. By assumption, the physical modes are simple and will therefore have a well-defined phase velocity which can be expanded as

$$\mathscr{V}_{\mathrm{p}}^{\delta}(K,\varepsilon)=\frac{\omega_0(K)}{|k|}+\xi^{\delta}(K)\varepsilon+\mathscr{O}(\varepsilon^2).$$

Here $\mathscr{V}_{\mathrm{p}}^{\delta}(K,\varepsilon)$ is a root of (32) and $\omega_0(K)$ is a root of (11). Correspondingly

$$\omega^{\delta}(k,d)=|k|\mathscr{V}_{\mathrm{p}}\left(\frac{k}{|k|},\frac{d}{|k|}\right)$$

is a root of (30).

Let $\omega_I=\Im\omega^{\delta}(k,d)$. A necessary condition for weakly stability is $\omega_I\geqslant 0$. Since (6) is a hyperbolic system $\Im\omega_0(K)=0$. Thus, at high frequencies, the sign of ω_I will be determined by the sign of $\Im\xi^{\delta}(K)$.

Now we expand (32) around $\varepsilon=0$ and arrive at

$$0=F_0(\omega_0(K),K_1,K_2)+\varepsilon\xi^{\delta}(K)\frac{\partial F_0(\omega_0(K),K_1,K_2)}{\partial\omega}+\mathrm{i}\varepsilon\frac{K_1}{\omega_0(K)-\mathrm{i}\delta}\frac{\partial F_0(\omega_0(K),K_1,K_2)}{\partial k_1}+\mathscr{O}(\varepsilon^2).$$

Neglecting the higher order terms we have

$$\Im\{\xi^{\delta}(K)\}=\Im\left\{-\mathrm{i}\left(\frac{\partial F_0(\omega_0(K),K_1,K_2)}{\partial\omega}\right)^{-1}\left(\frac{K_1}{\omega_0(K)-\mathrm{i}\delta}\frac{\partial F_0(\omega_0(K),K_1,K_2)}{\partial k_1}\right)\right\}.$$

We can identify the group velocity

$$\mathscr{V}_{\mathrm{g}}(K)=-\left(\frac{\partial F_0(\omega_0(K),K_1,K_2)}{\partial\omega}\right)^{-1}\nabla_kF_0(\omega_0(K),K_1,K_2),$$

and express $\xi^\delta(K)$ in terms of the first component of the slowness vector

$$S(K) = \frac{K}{\omega_0(K)},$$

and the first component of the group velocity $\mathscr{V}_{g1}(K)$,

$$\xi(K) = \mathrm{i}S_1(K)\mathscr{V}_{g1}(K)\frac{\omega_0(K)}{\omega_0(K) - \mathrm{i}\delta}.$$

We have

$$\Im\{\xi^\delta(K)\} = \frac{\omega_0(K)^2}{\omega_0(K)^2 + \delta^2} S_1(K)\mathscr{V}_{g1}(K). \tag{33}$$

Thus the sign of $\Im\{\xi^\delta(K)\}$ will not change when $\alpha_0 > 0$. This proves the following lemma.

Lemma 5. *Under the assumptions of Theorem 3, a necessary condition for stability of the PML model (27), with $\alpha_0 > 0$, is that all physical modes of (11) satisfy the condition on the orientation of the slowness curve (18). The condition is sufficient for stability of all physical modes with sufficiently high frequencies.*

The fact that the high frequency stability is not changed by α_0 implies that if we are able to choose α_0 so that the weak instabilities associated with material IV and V are removed, the model will be stable. Also, it again shows that the complex frequency shift cannot be used to remove the strong instabilities when materials of type III are considered.

Remark 6. The sign of $\Im\{\xi^\delta(K)\}$ could potentially be changed by adding a free parameter $\mathrm{i}\alpha_3 k_1$ in the modal solution (23). Such a parameter would enter into the layer equation as a derivative in the normal direction of the auxiliary variable. The matching properties and stability of such a model are under investigation.

If condition (19) is violated there will be high frequent non-physical modes that are unstable. For such cases α_0 will provide additional stability.

Lemma 7. *For sufficiently small damping d the parameter α_0 will stabilize the non-physical modes at high frequencies.*

Proof. For a fixed α_0 and $d = 0$ the dispersion relation (30), by homogeneity, can be written

$$(\mathscr{V}_p - \mathrm{i}\delta)^4 F_0(\mathscr{V}_p, K_1, K_2) = 0. \tag{34}$$

We know that the non-physical modes are continuous functions of ε and therefore can be expanded by a *Puiseux series* (see [24])

$$\mathscr{V}_p^\delta(K,\varepsilon) = \mathrm{i}\delta + \xi^\delta(K)\varepsilon^r + \mathrm{o}(\varepsilon^r), \quad r \in \mathbb{Q}^+.$$

If $r \geqslant 1$ then we know that the perturbed root $\mathscr{V}_p^\delta(K,\varepsilon)$ will have a positive imaginary part for sufficiently small ε i.e. it will be stable. Now assume that $r < 1$. By inserting the expansion into (32) we get

$$F_0(\xi^\delta(K)^2\varepsilon^{2r} + \mathrm{o}(\varepsilon^{2r}), K_1\xi^\delta(K)\varepsilon^r + \mathrm{o}(\varepsilon^r), K_2\xi^\delta(K)\varepsilon^r + \mathrm{o}(\varepsilon^r)) = 0.$$

For non-physical modes $F_0(\mathrm{i}\delta, k_1, k_2) \not\equiv 0$ since the physical modes are of order one. Therefore we can write

$$\begin{aligned}(\xi^\delta(K)\varepsilon^r)^4 F_0(\mathrm{i}\delta + \xi^\delta(K)\mathrm{o}(\varepsilon^r), K_1 + \mathrm{o}(1), K_2 + \mathrm{o}(1)) = 0 &\Rightarrow (\xi^\delta(K)\varepsilon^r)^4 F_0(\mathrm{i}\delta, K_1, K_2) + \mathrm{o}(1)\\ &\Rightarrow (\xi^\delta(K))^4 F_0(\mathrm{i}\delta, K_1, K_2) = 0.\end{aligned}$$

Thus we must have that $\xi^\delta(K) = 0$ which is a contradiction. Hence $r \geqslant 1$ and the lemma is proved. □

We note that the proof of Lemma 7 is analogous to the proof of Theorem 1 in [3], which considers the well-posedness of the general split-field model.

Remark 8. From Lemma 7 we see that we need $\varepsilon \ll \delta$ if $|\xi^{\delta}(K)| \gg 1$. In Section 6 we will present some numerical examples, which indicate that $\mathrm{d}|\xi^{\delta}(K)|$ is small, and therefore α_0 can also be chosen small. Our experience is that for most cases where (19) is violated this holds.

To fully understand the effect of α_0, it is necessary to analyze its influence on physical modes at intermediate frequencies. This we have not been able to do by analytical means. However, in Section 6 we will present a numerical analysis of the spectra of material V which indicates that α_0 can also be used to remove instabilities appearing when (20) or (21) are violated.

5.3. Well-posedness and hyperbolicity of the PML for orthotropic waves

In this section we will discuss the well-posedness and hyperbolicity of the modal PML for orthotropic waves. Freezing the coefficients and computing the principal part of the symbol for the modal PML (27), we get

$$P_m = \begin{pmatrix} \mathrm{i}k_1 A_1 + \mathrm{i}k_2 A_2 & 0 \\ -\mathrm{i}k_1 I & 0 \end{pmatrix}.$$

For the system (6), (7) one of the eigenvalues of $\mathrm{i}k_1 A_1 + \mathrm{i}k_2 A_2$ is identically zero and therefore P_m cannot be diagonalized. The problem is only weakly hyperbolic. From the proof of Lemmas 5 and 7 we know that the imaginary parts of the physical and non-physical modes are bounded. With $\omega_I = \Re\{\lambda(P(\mathrm{i}k))\}$ we know from (2) that the constant coefficient problem is weakly well-posed.

For a Cauchy problem with variable coefficients strong hyperbolicity implies well-posedness (the question of well-posedness can be determined by considering all "frozen coefficient" problems). However, if a constant-coefficient Cauchy problem is only weakly hyperbolic (and therefore only weakly well-posed), it is not sufficient to consider all its "frozen coefficient" problems to guarantee the well-posedness of the corresponding variable–coefficient problem.

In the context of PML it is clear that coefficients have spatial variation so from a mathematical point of view it is desirable that PML models should be strongly hyperbolic. This is not the case for the modal PML or for the split-field PML for orthotropic waves. However, we know of no numerical computations where there has been indications that a weakly well-posed PML model has become ill-posed when used with variable coefficients.

6. Numerical experiments

In this section we want to numerically investigate the stability and effectiveness of our new model. In the literature there exist few theoretical results on how the PML damping parameter d should be chosen for optimal performance. In general the error in a computation can be split into one part associated with the finite width of the layer, and one part associated with the numerical reflections due to the variability of d. The second part depends on the discretization.

In a first set of experiments (without the stabilizing parameter) we empirically determined a suitable strength and shape of the damping function d. These computations where done for all materials except III. The final time in these experiments was short relative to the growth rate of the unstable modes in materials IV and V.

Next we investigated to what extent $\alpha_0 > 0$ can be used to stabilize the model when used for materials IV and V. To do this we computed the eigenvalues of the symbol for the constant coefficient problem (27). From the theoretical investigations in Section 5.2 (for $\alpha_0 = 0$) we expected the physical modes at intermediate frequencies to be unstable for material V. For material IV we expected instabilities for non physical modes at high frequencies. The theoretical results where confirmed by the experiments.

Further, we performed simulations of the PML equations with constant d. In these simulations growth rates agreeing with the computed eigenvalues were observed. In another set of experiments we allowed d to vary spatially. Then, the observed growth rates were smaller, corresponding to smaller effective damping.

By further investigations of the eigenvalues of the symbol we found, as expected, that the high frequency instabilities in the non-physical modes (material IV) could be removed by a suitably chosen α_0. Moreover, we found that the instabilities at intermediate frequencies for physical modes could also be stabilized. In both cases we determined suitable numerical values for α_0 with a typical value of d from the first set of experiments. With our stabilized PML we revisited the first experiment and found that the change in performance was negligible.

Finally we compared the performance of the PML with characteristic variables.

6.1. Damping parameter

In our first test problem we solve Eqs. (6) and (7) on the computational domain consisting of the square $(x_1, x_2) \in [-10, 10] \times [-10, 10]$. As a non-reflecting boundary condition we add the layer $(x_1, x_2) \in [10, 12.9] \times [-10, 10]$, where we solve the PML equation (27) without the stabilizing parameter.

The damping is chosen as the function

$$d(x_1) = \begin{cases} d_{\max}\left(1 - \frac{(x-11.45)^2}{1.45}\right)^p & 10 < x < 12.9,\ p = 4, \\ 0 & x \leqslant 10. \end{cases} \tag{35}$$

See Fig. 3 for a graphical description of the problem setup and the shape of the damping function.

To generate a wave we force the first component of the right-hand side of (6)–(7) by the pulse

$$f = (2\pi^2(0.9t-1)^2 - 1)\mathrm{e}^{-\pi^2(0.9t-1)^2} g(x_1, x_2), \quad g(x_1, x_2) = \frac{1}{0.5^2}\mathrm{e}^{-7\frac{(x_1)^2+(x_2)^2}{0.5^2}}.$$

We use periodic boundary conditions in both directions.

To solve the problem numerically we introduce the grid $x_{1,i} = ih_1,\ i = -N_1/2, \ldots, 0, \ldots, N_1/2 + N_l$, $x_{2,j} = jh_2,\ j = 0, \pm 1, \ldots, \pm N_2/2$. Here $h_1 = 20/N_1$ and $h_2 = 20/N_2$ is the grid spacing in each direction. The integers N_1, N_2 and N_l controls the number of grid points in each direction and in the layer.

We approximate the spatial derivatives with the standard eighth order centered difference stencil. For the integration in time we use the standard fourth order Runge–Kutta method.

To measure the error we compute a reference solution. This is done by solving Eqs. (6),(7) on a larger domain, consisting of the rectangle $(x_1, x_2) \in [-70, 70] \times [-10, 10]$. In all experiments we measure the relative error

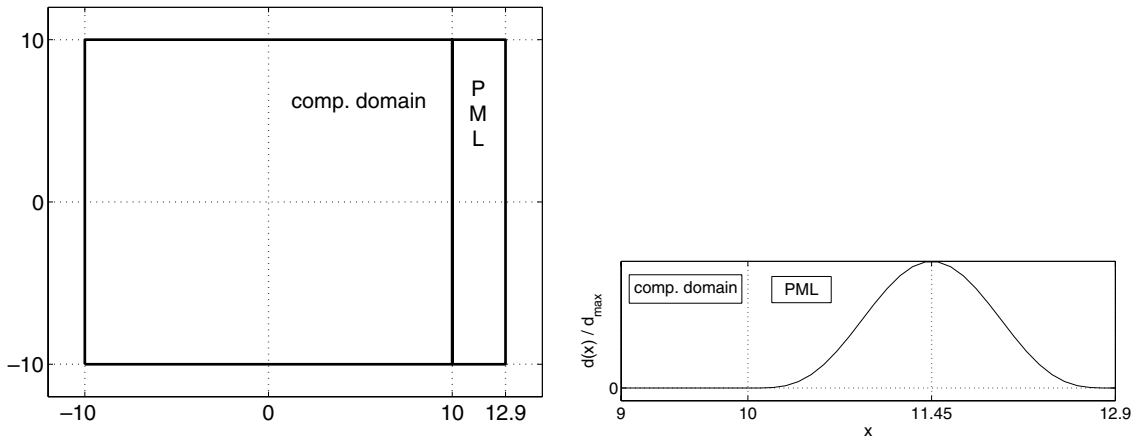

Fig. 3. Computational domain and shape of damping function. Due to the periodic boundary conditions this setup corresponds to having a layer on each side with monotonically increasing damping functions.

$$\frac{\left\| \sqrt{v_{1,\mathrm{pml}}^2 + v_{2,\mathrm{pml}}^2} - \sqrt{v_{1,\mathrm{ref}}^2 + v_{2,\mathrm{ref}}^2} \right\|_2}{\left\| \sqrt{v_{1,\mathrm{ref}}^2 + v_{2,\mathrm{ref}}^2} \right\|_2}. \tag{36}$$

To determine a suitable strength for the damping of the PML we compute solutions (and errors) for several different values of $d_{\max}$ and the parameter, p in (35). In our computations we use $N_1 = N_2 = 200$ and $N_l = 29$. We find, empirically, that a suitable choice of p is 4 for all materials. For all tested materials, except material I, the optimal value of $d_{\max}$ is in the interval 80–180. For material I it is smaller, 20–40. In material I the quasi-transverse wave is much slower than in the other materials and we believe this is the reason for the smaller value of $d_{\max}$. In Figs. 4 and 5 the relative error for different values of $d_{\max}$ (with $p = 8$) is plotted for different materials.

6.2. Stabilizing the PML

In this section we only consider the layer $(x_1, x_2) \in [10, 12.9] \times [-10, 10]$, where we solve the PML equation (27) for either material IV or V.

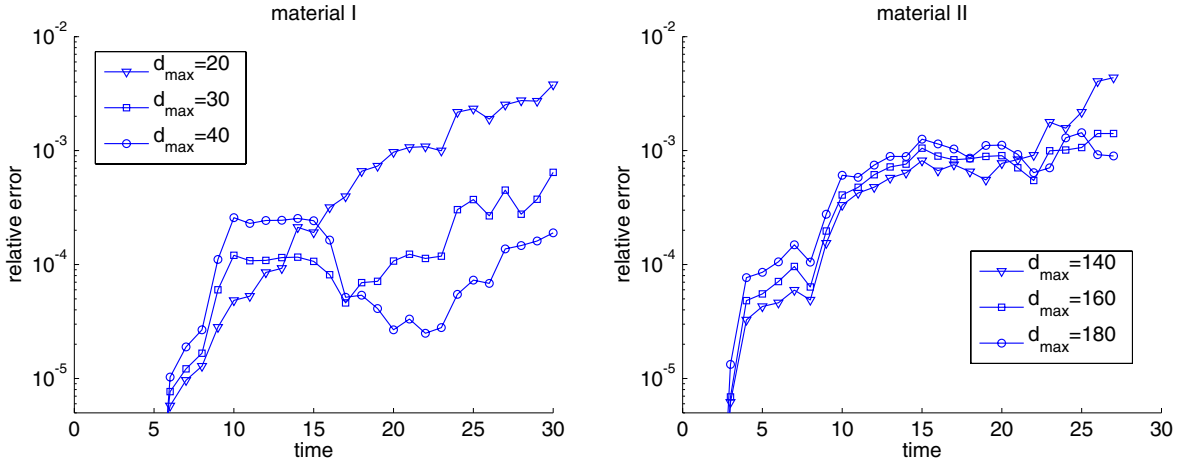

Fig. 4. Relative error.

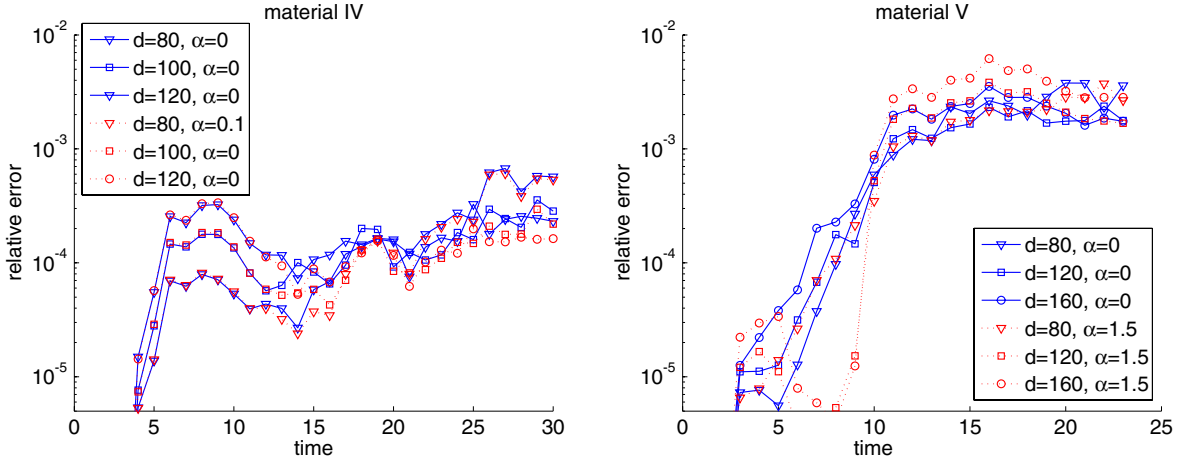

Fig. 5. Relative error. Here d denotes $d_{\max}$ and α denotes α_0.

6.2.1. The discrete spectrum

6.2.1.1. Material IV. Based on the experiments in the previous section, a typical value of $d_{\max}$ is 80. When d is constant we can compute the eigenvalues λ of the symbol

$$P(k_1, k_2) = \begin{bmatrix} \mathrm{i}k_1 A_1 + \mathrm{i}k_2 A_2 & dA_1 \\ -\mathrm{i}k_1 I & -(d+\alpha_0)I \end{bmatrix}, \tag{37}$$

numerically, for discrete frequencies. In the layer $(x_1, x_2) \in [10, 12.9] \times [-10, 10]$ (on the grid described in the previous section), we can represent the discrete frequencies $k_1 = \pm s\pi/2.9$, $s = 0,1, \ldots, N_l$, $k_2 = \pm s\pi/20$, $s = 0, 1, \ldots, N_2$.

We expect the unstable modes for material IV to appear at high frequencies relative to the size of the damping, i.e. for $d < |k|$. For example when we compute the discrete spectrum with $d = 80$, $N_l = 29$ and $N_2 = 200$ there are no unstable modes. However, when we increase the number of grid points to $N_l = 290$ and $N_2 = 500$ we observe the growing modes displayed in Fig. 6.

In Fig. 6 the largest real part of the eigenvalues of (37) is plotted for two values of d. To the left $d = 80$ and to the right $d = 5$. Computing the same quantity for several other values of d, we typically find that the unstable modes appear when $k_1 \approx d$. This is also the case for the examples in Fig. 6. In the Figure we see that the unstable eigenvalues approach a maximum value as k_1 and k_2 increase. This is expected since we know from Section 5.3 that the problem is weakly well-posed, i.e. $\max_j \Re\lambda_j < \kappa$.

We know from Eq. (34) that non-physical modes are shifted with α_0 into the stable half plane when $d = 0$. Making experiments where we gradually increase $\alpha_0 > 0$ we find that, with large d, we can still stabilize the unstable eigenvalues. For material IV we conclude that the needed size of α_0 is about equal to the maximum growth rate. In the examples with $d = 80$ and $d = 5$, $\alpha_0 = 0.4$ and $\alpha_0 = 0.1$ respectively, suffices.

It should be noted that when d increases, so does the growth rate and along with it the size of α_0. However, in a real computation there is an upper bound on $d_{\max}$ (due to numerical reflections), and thus an upper bound on α_0.

6.2.1.2. Material V. For material V we expect the unstable modes to be physical modes at intermediate frequencies. High frequencies of these modes should be stable since the geometrical condition (18) is fulfilled.

In the left subfigure in Fig. 7 we plot the level contours of the largest real part of the eigenvalues of (37) as a function of k_1 and k_2. This is done for three values of d, 20, 40 and 80 and $\alpha_0 = 0$. As expected there are unstable modes at intermediate frequencies, $|k| < d$.

In Section 5.2 we used perturbation techniques that require $|k| \gg d$, and could anticipate a linear shift of the unstable modes for material IV. For material V we have instabilities at intermediate frequencies and cannot use these techniques. However, when we gradually increase α_0, we find that the unstable modes are

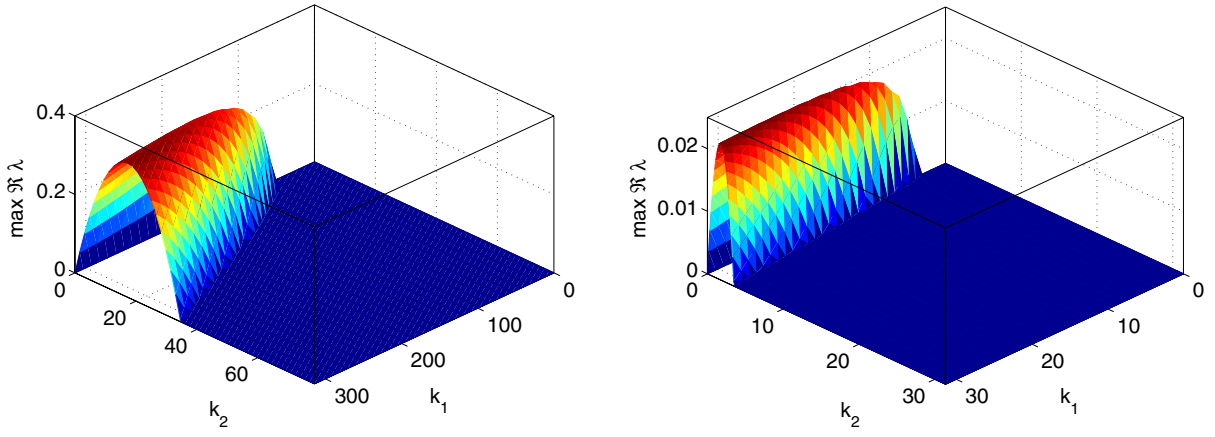

Fig. 6. $\max_j \Re\lambda_j$ for material IV. To the left $d = 80$ constant and $\alpha = 0$. To the right $d = 5$ constant and $\alpha = 0$. Note the orientation of the axis. The unstable modes start at $k_1 \approx d$.

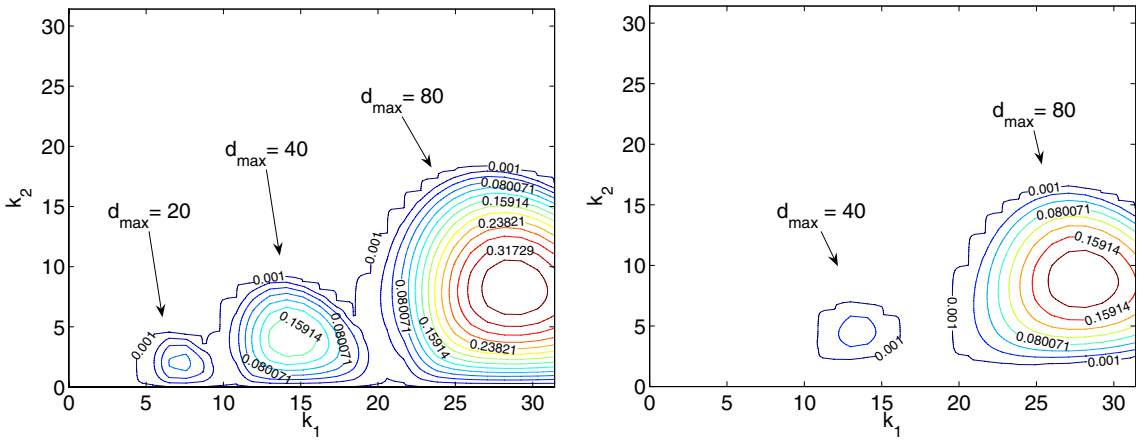

Fig. 7. $\max_j \Re\lambda_j$ for material V. The pictures display the contours when $d = 20, 40, 80$ and $\alpha_0 = 0$ (left) or $\alpha_0 = 0.5$ (right).

stabilized. For material V the α_0 needed for stability is about four times the growth rate. In the right subfigure in Fig. 7 we have plotted contours of the largest real part of the eigenvalues of (37) for d, 20, 40 and 80, but now with $\alpha_0 = 0.5$. Already, the smallest "bump" has been removed, but we need $\alpha_0 = 1.5$ to remove all of them.

6.2.2. Time dependent simulations

Using the same numerical scheme as in Section 6.1, we solve the PML equation (27) in the layer $(x_1, x_2) \in [10, 12.9] \times [-10, 10]$.

First we solve for material IV. In all simulations we excluded the forcing and start the simulations with the initial data

$$v_1(x_1, x_2, 0) = v_2(x_1, x_2, 0) = \sin\left(\frac{\eta_1 \pi x_1}{2.9} + \frac{\eta_2 \pi x_2}{20}\right). \tag{38}$$

We take $\eta_1 = 16$ and $\eta_2 = 6$, corresponding to an eigenvalue with real part 0.022 when $d = 5$ and real part 0 when $d = 80$. We take $N_2 = 200$ and $N_l = 29$. For all test cases we measure the L^2 norm of $\sqrt{v_1^2 + v_2^2}$.

The results are displayed in the left subfigure of Fig. 8. The solid line is a computation with constant $d = 5$. The solution grows fast, and by a least square fitting we find the growth rate to be 0.0213. As a reference we plot the function $e^{0.0213t}$ (the dotted line). The solid line with circles is a computation with constant $d = 5$ and

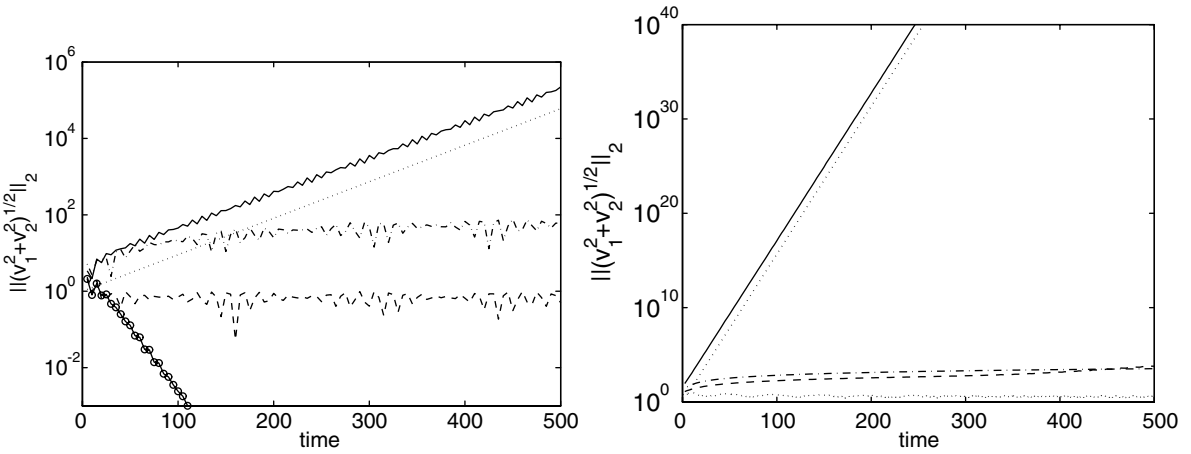

Fig. 8. The figure displays the L^2 norm of $\sqrt{v_1^2 + v_2^2}$ for different values of parameters (see the text for details). To the left is material IV and to the right is material V.

$\alpha_0 = 0.1$. As expected the mode is stabilized. In this case the solutions decreases fast until it saturates at 10^{-12}. The dashed–dotted line is a computation where $d = d(x_1)$ and $\alpha_1 = 0$. The damping d is the function (35) with $d_{\max} = 80$ and $p = 4$. This solution grows but with a slower rate, 0.00372. Finally, the dashed line is a computation with $d_{\max} = 80$ and $p = 4$ and $\alpha_0 = 0.1$. This solution is stable.

Next we solve for material V. We use the initial data (38) but now with $\eta_1 = 25$ and $\eta_2 = 59$. This corresponds to an eigenvalue with real part 0.362 with constant $d = 80$. In this experiment we use two resolutions, one coarser with $N_2 = 200$ and $N_l = 29$, and one finer with $N_2 = 400$ and $N_l = 58$.

The results are displayed in the right subfigure of Fig. 8. The dash-dotted line is a computation with the coarser grid and constant $d = 80$. This solution grows, but with a slower rate, 0.0057, than expected. On the coarser grid the initial data is not well resolved and we argue that slower growth rate is due to discrete numerical effects. Supporting this argument is the solid line obtained from a computation with the finer grid with constant $d = 80$. This solution grows with the rate, 0.3607, which is very close to the expected rate, 0.362. The dotted line is the function $e^{0.3607t}$, added for reference.

The dashed line is a computation on the finer grid with $d_{\max} = 80$ and $p = 4$. It does grow, although rather slowly, 0.0045. In general, when d varies spatially, the growth rate decreases. Finally, the lower dotted line is a computation with $d_{\max} = 80$ and $p = 4$, together with $\alpha_0 = 1.5$. The solution is stable and decays slowly -0.001.

Here we have only presented the results for a specific initial data. We have also performed experiments with several other sets of initial data and with different forcing both for the constant coefficient problem and for the variable coefficient problems. They all behave similarly.

As a final test we take $\alpha_0 = 0.1$ for material IV and $\alpha_0 = 1.5$ for material V in the test problem from Section 6.1. In Fig. 5 the results are shown as the dotted lines. As can be seen there is little effect on the efficiency when $\alpha_0 > 0$.

6.3. Comparison with characteristic boundary conditions

Finally we present some experiments displaying the efficiency of the modal PML compared to the simplest boundary procedure. To do this we compute solutions for a problem on the computational domain defined as the square $(x_1, x_2) \in [-10, 10] \times [-10, 10]$. On the computational domain we solve (6), (7). We force the v_1 component in the solution by the pulse

$$f = (2\pi^2(t-1)^2 - 1)e^{-\pi^2(t-1)^2} g(x_1, x_2), \quad g(x_1, x_2) = \frac{1}{0.5^2} e^{-7\frac{(x_1+8)^2+(x_2-8)^2}{0.5^2}}.$$

We surround the computational domain by a layer of width 2. The damping function, d, is chosen as a monotone fourth order polynomial taking the maximal value 50 at the outermost boundary.

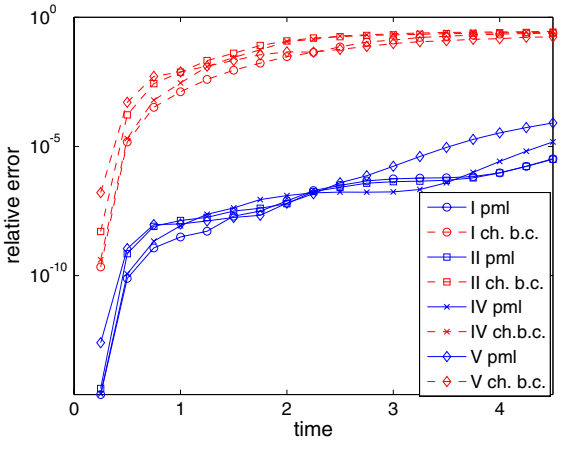

Fig. 9. Comparison of the error for the modal PML and characteristic boundary conditions.

As comparison we compute the solution to the same problem but the computational domain is now terminated with characteristic boundary conditions. That is, we extrapolate outgoing characteristic variables and put incoming characteristic variables to zero (see e.g. [25]). The errors are obtained by computing a reference solution on a larger computational domain. This is done for materials I, II, IV and V and the results can be found in Fig. 9. In Fig. 10 $\sqrt{v_1^2 + v_2^2}$ is plotted at $t = 5, 10, 15, 20$ for material I. The computational domain is closed either with the modal PML or with characteristic boundary conditions. When the modal PML is used, no reflections are seen but with characteristic boundary conditions reflections, polluting the solution, can be seen. Similar results where obtained for materials II, IV and V.

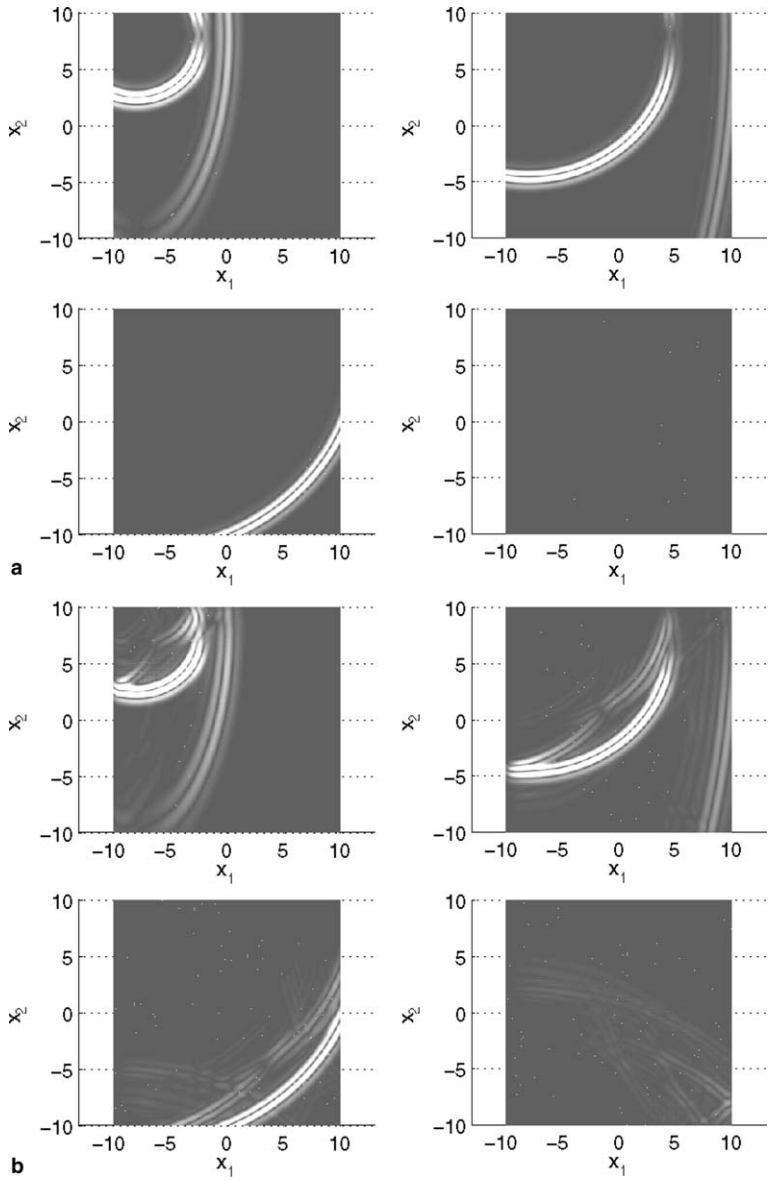

Fig. 10. $\sqrt{v_1^2 + v_2^2}$ at time $t = 5, 10, 15, 20$ is plotted with modal PML and characteristic boundary conditions: (a) material I with PML; (b) material I with ch. b.c.

7. Summary

In this paper we considered the equations of elasticity in an anisotropic material. We have studied the same five materials as in [3]. These materials where chosen to illustrate different types of behavior for the split-field PML. Using the split-field PML together with three of these materials (III, IV, V), results in a model that supports exponentially growing solutions. With our new model, which includes an additional parameter, two of these three (material IV and V) could be stabilized.

We have presented new theoretical results. First we established a formal equivalence between the split-field PML and the modal PML without the stabilizing parameter. We then showed that the stability was improved by the new parameter. In particular we showed that the instability for material IV can be removed. Our analysis also showed that one of the instabilities (III) cannot be stabilized by the current model.

We also presented numerical experiments that illustrate the theoretical results. Further, the experiments showed that material V also be stabilized by the new parameter. Empirically we determined suitable numerical values for the damping parameter. For these values we established the size of the stabilizing parameter.

References

[1] J. Bérenger, A perfectly matched layer for the absorption of electromagnetic waves, J. Comput. Phys. 114 (1994) 185.
[2] F. Collino, C. Tsogka, Application of the PML absorbing layer model to the linear elastodynamic problem in anisotropic heterogeneous media, Geophysics 66 (1) (2001) 294–307.
[3] E. Bécache, S. Fauqueux, P. Joly, Stability of perfectly matched layers, group velocities and anisotropic waves, J. Comput. Phys. 188 (2003) 399–433.
[4] F.Q. Hu, On absorbing boundary conditions for linearized Euler equations by a perfectly matched layer, J. Comput. Phys. 129 (1996) 201–209.
[5] I. Navon, B. Neta, M. Hussaini, A perfectly matched layer approach to the linearized shallow water equations models, Monthly Weather Rev. 132 (2004) 1369–1378.
[6] E. Bécache, P. Joly, On the analysis of Bérenger's perfectly matched layers for Maxwell's equations, Math. Mod. Numer. Anal. 36 (1) (2002) 87–119.
[7] E. Bécache, P. Petropoulos, S. Gedney, On the long-time behavior of unsplit perfectly matched layers, IEEE Trans. Antennas Propagat. 52 (2004) 1335–1342.
[8] S. Abarbanel, D. Stanescu, M. Hussaini, Unsplit variables perfectly matched layers for the shallow water equations with Coriolis forces, Computat. Geosci. 7 (2003) 275–294.
[9] S. Abarbanel, D. Gottlieb, J. Hesthaven, Well-posed perfectly matched layers for advective acoustics, J. Comput. Phys. 154 (1999) 266–283.
[10] S. Abarbanel, D. Gottlieb, A mathematical analysis of the PML method, J. Comput. Phys. 134 (1997) 357.
[11] S. Abarbanel, D. Gottlieb, On the construction and analysis of absorbing layers in CEM, Appl. Numer. Math. 27 (1998) 331–340.
[12] S. Abarbanel, D. Gottlieb, J. Hesthaven, Long time behaviour of the perfectly matched layer equations in computational electromagnetics, J. Sci. Comput. 17 (1–4) (2002) 405–422.
[13] F.D. Hastings, J.B. Schneider, S.L. Broschat, Application of the perfectly matched layer (PML) absorbing boundary condition to elastic wave propagation, J. Acoust. Soc. Am. 100 (5) (1996) 3061–3069.
[14] D. Komatitsch, J. Tromp, A perfectly matched layer absorbing boundary condition for the second-order seismic wave equation, Geophys J. Int. 154 (2003) 146–153.
[15] W. Chew, Q.H. Liu, Perfectly matched layers for elastodynamics: a new absorbing boundary condition, J. Comput. Acoust. 4 (4) (1996) 341–359.
[16] T. Hagstrom, Perfectly matched layers for hyperbolic systems with applications to the linearized Euler equations, in: Cohen et al. (Eds.), Mathematical and Numerical Aspects of Wave Propagation, Proceedings Waves2003, Springer-Verlag, 2003, pp. 125–129.
[17] H.-O. Kreiss, J. Lorenz, Initial-Boundary Value Problems and the Navier–Stokes Equations, Academic Press Inc., 1989.
[18] A.I. Beltzer, Acoustics of Solids, Springer-Verlag, 1988, ISBN 0-387-18888-6.
[19] D. Appelö, T. Hagstrom, Sufficient conditions for the construction of a stable PML for a general 2×2 symmetric hyperbolic system, submitted to Hyperbolic Problems: Theory, Numerics, Applications, in: Proceedings of the Tenth International Conference on Hyperbolic Problems, 2004.
[20] J. Diaz, P. Joly, Stabilized perfectly matched layer for advective acoustics, in: Cohen (Ed.), Mathematical and Numerical Aspects of Wave Propagation, Proceedings Waves2003, Springer-Verlag, 2003, pp. 115–119.
[21] F.Q. Hu, A stable perfectly matched layer for linearized Euler equations in unsplit physical variables, J. Comput. Phys. 173 (2001) 455–480.
[22] T. Hagstrom, New results on absorbing layers and radiation boundary conditions, in: Ch.T. Hagstrom Topics in Computational Wave Propagation, in: M. Ainsworth, P. Davies, D. Duncan, P. Martin, B. Rynne (Eds.), Lecture Notes in Computational Science and Engineering, vol. 31, Springer-Verlag, New York, 2003, pp. 1–42.

[23] M. Kuzuoglu, R. Mittra, Frequently dependence of the constitutive parameters of causal perfectly matched anisotropic absorbers, IEEE Microwave and Guided Letters 6 (12) (1996) 447–449.
[24] T. Kato, Perturbation Theory for Linear Operators, Springer-Verlag, 1966.
[25] B. Gustafsson, H.-O. Kreiss, J. Oliger, Time Dependent Problems and Difference Methods, John Wiley, New York, 1995.